Version of Record: https://www.sciencedirect.com/science/article/pii/S2352492822012089
Manuscript_ee5c9b6b60099b9fd3cd67b45c5c812e

Effect of atomic size mismatch and chemical complexity on the local lattice distortion of BCC solid solution alloys

F.X. Zhang[1], Hong-Quan Song[2,1]

[1]*Songshan Lake Materials Laboratory, Dongguan 523808, China*

[2]*College of Physics and Telecommunication Engineering, Zhoukou Normal University, Zhoukou 466001, China*

Abstract

The effects of atomic size mismatch and chemical complexity on the local lattice distortion of solid-solution alloys VNbTa, TiVNbMo, TiVNbMoTa and TiVNbMoTaWRe with body-centered cubic (BCC) structure are quantitatively studied with time-of-flight neutron total scattering, extended X-ray absorption fine structure (EXAFS) measurements and first principles calculations. Neutron atomic pair distribution function (PDF) measurements found that the local lattice distortion in the ternary solid-solution alloy VNbTa is 1.1%, obviously larger than that of the most complicated solid-solution alloy (0.27% for TiVNbMoTaWRe). Our results suggested that atomic size mismatch in high entropy alloys is more critical to the local lattice distortion than chemical complexity. Both EXAFS analysis and theoretical calculations indicate that there is a maximum of ~4% difference between the bonding length of different atomic pairs in VNbTa.

1. Introduction

High entropy alloys (HEAs) are solid-solutions of multi-principal elements with nearly equiatomic chemical composition [1–3]. It is believed that the high configurational entropy has a significant effect on the Gibbs' energy of crystalline phase, which stabilizes solid-solutions rather than intermetallic phases [4–6]. Due to the atomic size mismatch, local lattice distortion is believed to be one of the main structural characters of HEAs [1,3,7,8]. Numerous investigations have shown that lattice strain yielding from local lattice distortion plays a key role to the structural stability, precipitation, microstructure, formation and evolution of defects, which affect the integrated mechanical properties of HEAs [9–13]. Generally, the localized distortion around the solute atoms interacts elastically with the dislocations through the material, resulting in solid-solution strengthening [14–16]. The most studied medium-entropy alloys of CoCrNi, CoCrFeNi are stable FCC solid-solutions, while CoCrFeMnNi is not so stable and precipitation occurs when it is annealed at elevated temperatures [17]. Due to the chemical short-range order, however, the formation of intermetallic phases becomes more likely as the number of alloying elements increases. The lattice distortion of HEAs arises from not only atomic size mismatch, but also the differences in the crystal structure and bonding preferences of alloying elements present.

Lattice distortion in HEAs was generally described by the parameter of atomic size mismatch before [6,18]. Atomic size mismatch (δ) is an empirical concept borrowed from metallic glass, which describes the glass forming ability. The atomic size mismatch is generally estimated as [18]

$$\delta = 100\sqrt{\sum_{i=1}^{n} c_i (1-\frac{r_i}{\overline{r}})^2}$$

where $\overline{r} = \sum_{i=1}^{N} c_i r_i$, with c_i and r_i being the atomic percentage and atomic radius of the individual alloy component, respectively. Experimental results suggested that larger atomic size mismatch (δ>11%) favors the formation of metallic glass, and HEAs have less δ values [18]. However, the estimation of δ is very rough because the

atomic size of elements depends on the crystal structure and the atomic radius in alloys is even not strictly defined. In recent years, an experimental method based on total scattering has been built [7,19,20] which can quantitatively measure the lattice distortion in HEAs, and the results indicated that the lattice distortion in HEAs is localized in a distance of 2-3 unit cells. Experimental results also suggested that the lattice distortion in most HEAs was over estimated with atomic size mismatch parameter, especially to the FCC solid solution alloys [7,21,22]. Chemical complexity has also effects on the structural disorder, which can introduce additional lattice vibrations at 0 K [23] and local lattice distortion. X-ray diffraction has found structural distortion in some refractory solid solution alloys with BCC structure [24], and the lattice distortion of some Zr- and Hf-bearing HEAs was also studied by X-ray total scattering method [20]. However, the synergetic effects of atomic size mismatch and chemical complexity on the lattice distortion of HEAs are not systematically studied before. In this paper, the effects of atomic size mismatch and chemical complexity on the lattice distortion in four BCC solid-solution alloys with different chemical complexity are quantitatively investigated by using time-of-flight total neutron scattering, extended X-ray absorption fine structure measurements and theoretical calculations.

2. Experimental details and calculation methods

Solid-solution alloy ingots were prepared by arc melting of high purity element mixtures for more than 5 times and casted in a copper mold. The neutron total scattering measurements were conducted at NOMAD station, Spallation Neutron Source at Oak Ridge National Laboratory with time-of-flight neutron source, the measured PDFs were refined with random bcc structure models using PDFGui software [25]. EXAFS spectra were collected at beam 6-BM-M, National Synchrotron Light Source II at Brookhaven National Laboratory. The EXAFS at the K-edge of each element was measured in fluorescence mode and the energy was calibrated with the known energies of absorption edge of pure metal foils. The fluorescence X-ray was collected in grazing exit mode with angle of 2~5 degrees in order to reduce

self-absorption. The analysis of the Fourier Transforms (FTs) of EXAFS and fitting were conducted using Demeter software in k range of 3-13 $Å^{-1}$ [26].

The local structure of the BCC solid solution alloys was also studied by first-principles calculation based on density functional theory by constructing a supercell model. Vienna *ab initio* simulation package (VASP) software was employed to optimize the lattice structures and obtain system energies. The interaction between ions and electrons was processed by the Projector Augmented Wave (PAW) method [27]. The exchange-correlation potential was adopted the Perdew–Burke–Ernzerhof (PBE) [28] method under the Generalized Gradient Approximation (GGA). The plane wave cutoff energy was set to 400 eV, and the total energy convergence criterion was set to $1x10^{-5}$ eV/cell. The conjugate gradient method was adopted for the processing of the structure relaxation, and the force components were relaxed to less $1.0x10^{-2}$ eV/Å. The 3 × 2 × 2 (2 × 2 × 1) Monkhorst-pack k-point mesh and the Methfessel-Paxton technique were used for VNbTa, TiVNbMo and TiVNbMoTa (TiVNbMoTaWRe) supercells, which are constructed by 3 × 4 × 5 (3 × 3 × 7) supercell with BCC crystal structure. The Gaussian Smearing method was adopted to distribute the electron near the Fermi level for increasing the convergence speed. The valence electron configurations of Ti, V, Nb, Mo, Ta, W and Re were $3d^24s^2$, $3d^34s^2$, $4s^24p^64d^35s^2$, $4d^45s^2$, $5d^36s^2$, $5d^46s^2$ and $5d^56s^2$ respectively. The supercell structures in the present work were built by similar atomic environment (SAE) software [29]. Fig. 1a shows the crystal structure of VNbTa supercell with 54 atoms which positions have been optimized by the SAE method, and the corresponding pair correlation function of VNbTa MEAs is demonstrated in Fig. 1b.

3. Results and Discussion

3.1 Local lattice distortion measured with time-of-light neutron

Unlike FCC solid-solution alloys, BCC is not a close-packed structure. Precious X-ray total scattering measurements [20] have revealed that the BCC solid-solution alloys generally have much larger local lattice distortion (LLD) than the known FCC solid-solution alloys, except CoCrFeMnNiPd [7,21]. Zr- and Hf-bearing

solid-solution alloys with BCC structure have anomalously larger local lattice distortion of more than 2% [20]. The BCC solid-solution alloys can contain metal elements from 3d to 5d. It is interesting to compare the effect of different d-shell electrons on the local structure of solid-solution alloys. Fig. 2 shows the atomic pair distribution function (PDF) profile of VNbTa measured with TOF neutron total scattering techniques. With a randomly distributed structure model, the fitting shown as the solid line yields a lattice constant of 3.2290 Å. However, the first two peaks corresponding to the 1st and 2nd nearest neighbors, cannot be well fitted and their d-values obviously shifted from the expectation, which suggests a severely local lattice distortion in one unit cell range. Since the lattice is severely locally distorted, we fit the PDF profile in 3 different regions separately, i) local (within one unit cell <4 Å); ii) long-range (beyond 3-unit cells) and iii) the intermediate region. As shown in the bottom panel of Fig. 2, the fitting is much improved. The lattice constant in the long-range region is 3.2287 Å, very close to the whole range fitting. We define the relative change between the lattice derived from the fitting in different regions and that from total profile fitting as the lattice strain, similar with the LLD concept used before [7,19,20,22]. The fitting in local region yields a lattice constant of 3.265 Å and the corresponding strain is 1.11%. This is larger than that of all the HEAs with FCC structure. The lattice strain exists very locally in the lattice of VNbTa solid-solution alloy, and the strain in the medium-range (1-3 unit cell) drops quickly to 0.7%. The larger local lattice strain in BCC solid solution alloys than the FCC alloys is easy to be understood because BCC is not a close-packed structure and atoms in the unit cell may have more “free” space to adjust their positions which can minimize the total lattice energy.

In order to check the effect of chemical complexity on the local lattice distortion, we measured other three HEAs with different chemical compositions TiVNbMo, TiVNbMoTa and TiVNbMoTaWRe. Fig. 3 shows the observed PDF of TiVNbMoTaWRe HEAs fitted with a random distributed structural model in different space range. It is obvious that the fitting of the first two peaks in this 7 principle

element HEA are better than that in the ternary system. Similar analysis indicated that the maximum local lattice strain in this HEA is 0.27%, only 1/4 of the ternary alloy. Similar fitting was performed for the 4 and 5-element alloys and the lattice strain is shown in Fig. 4. It is obvious that the local lattice strain decreases with the increase of chemical complexity, from 1.11% in the ternary alloy to 0.69% and 0.61% in the 4- and 5-element alloys, respectively, and to the smallest of 0.27% in the 7-element alloy.

It is interesting to compare the local lattice strain based on PDF measurements and the estimated lattice mismatch with the empirical formula and atomic sizes. Table 1 illustrates the calculated and measured local lattice distortion, and estimated atomic size mismatch. The calculated local lattice distortion is defined as terms of the change of atomic coordinate position with respect to the ideal lattice sites

$$\Delta d = \frac{1}{N}\sum_i \sqrt{(x_i - x_i')^2 + (y_i - y_i')^2 + (z_i - z_i')^2}$$

where N is the number of atoms, and (x_i, y_i, z_i) and (x_i', y_i', z_i') are the reduced coordinates of the ideal and distorted positions of each atom for individual alloy component. Comparing the 4 HEAs, the most chemically complicated 7-element alloy has the smallest values of LLD, which is in agreement with estimated δ and Δd values. The estimated atomic size mismatch δ for the 4 studied HEAs have similar values. However, the measured LLD and the corresponding δ values of all the alloys have big difference, and the atomic size mismatch obviously overestimated (3 to 12 times) the local lattice distortion to the alloys with 4 and more elements. Our results indicated that chemical complexity of high entropy alloys is close related to local lattice distortion, but is not a must. Atomic size mismatch is an easy way to estimate the lattice distortion, while PDF is a quantitative method which can accurately measure the local lattice strain of HEAs.

Table 1 The maximum local lattice distortion (LLD) measured by neutron PDF, the estimated atomic size mismatch δ, calculated lattice constant (a), bulk modulus E and lattice distortion quantity (Δd) of HEAs

HEAs	VNbTa	TiVNbMo	TiVNbMoTa	TiVNbMoTaWRe
LLD*	1.11%	0.69%	0.61%	0.27%
δ	3.845%	4.076%	3.781%	3.353%
Δd (Å)	0.0955	0.1126	0.0937	0.0586
a (Å)	3.2197	3.1640	3.1992	3.1692
E (GPa)	180.8	178.6	182.2	228.8

3.2 Atomic pair distance measured with EXAFS

The local lattice distortion in HEAs is due to the position offset of individual atoms from the ideal lattice sites, and the interatomic distance of individual pairs is thus a little different. This reflects the broadening of Bragg peaks in the XRD or neutron diffraction profiles. However, normal diffraction and total scattering methods are difficult to provide details of individual atomic pair distance in HEAs. The interatomic distance can be either calculated from first-principles or measured by EXAFS with certain simplified structure models [30]. Fig. 4 shows the k^2-weighted FTs of EXAFS at the K-edge of V and Nb and L_3-edge of Ta in VNbTa solid-solution alloy. The dotted and solid lines are observed and fitted with a randomly distributed solid-solution structure model with 4 shells of neighbors. The reciprocal space k range is 3-11, 2.4-12 and 3.6-14 for the K-edge of V and Nb, and L3-edge of Ta, respectively. The interatomic distance of individual pairs are listed in Table 2. The average interatomic distance around core atoms of V, Nb and Ta is 2.77 Å, 2.82 Å and 2.85 Å, respectively, which is in good agreement with the trend of expected atomic sizes.

The fitting of FTs for alloys of TiVNbMo, TiVNbMoTa and TiVNbMoTaWRe is difficult because of too many fitting parameters due to the chemical complexity. In order to obtain a reasonable result, the structure model is simplified as a ternary-like systems based on the atomic weight, for example, the seven elements in the most complicated HEA was simplified as 3 groups of (TiV)(NbMo)(TaWRe). The deducted interatomic distance of different pairs in the BCC solid-solution alloys are illustrated in Table 2. The trend of bonding distance between different pairs is in generally good agreement with the sum of atomic size, which suggests that our simplification of structural models for FTs fitting is reasonable.

3.3 Theoretical calculations

To understand the details of the lattice distortion in these solid solution alloys, the relaxed crystal structures were obtained by using the first principles calculations. The structures of HEAs were built by similar atomic environment (SAE) software [29,31], and the structure screening is conducted by the software according to the pair correlation functions up to the third nearest neighboring atomic pairs (see Fig. 1b). In order to obtain the stable structures, all the structures undergo the relaxation process for releasing stress, and the system energies reach the minimum. The calculated distance of different atomic pairs in VNbTa alloy are listed in Fig. 6 together with those derived from EXAFS measurements, and the calculated values are generally fit well with the measured ones. The calculated bond lengths in other HEAs are shown in Figs. s1-s3 as supplementary. Though the EXAFS analysis of other BCC solid solution alloys used simplified structure models, the derived interatomic distances are in general agreement with the calculated values. Under the influence of alloying, the most homoatomic distances in the alloy is quite distinct from that in a pure metal (listed in Tables s1, s2). For examples, the homoatomic distances of V-V (Nb-Nb and/or Ta-Ta) in the four alloys are clearly larger (smaller) than that in pure metals. Instead, the impact acting on the homoatomic distances of Ti-Ti were relatively small in the TiVNbMo, TiVNbMoTa and TiVNbMoTaWRe alloys. Unlike the case of V-V and Ti-Ti, the average homoatomic distances of Mo-Mo were more complex, which became small in the TiVNbMo and TiVNbMoTaWRe alloys, and slightly large in TiVNbMoTa. To most heteroatomic distances, the values are between the corresponding homoatomic distances. The results indicated that the alloying atomic radius were significantly different with that in the pure metals. The difference of homoatomic distance in pure metal and solid solution alloys are attributed to the charge transfer between atoms with different electronegativity [20,32]. In fact, the charge transfers can be calculated according to Bader topological analysis [33]. Charge transfer between atoms strongly interrelates with atomic distribution, which changes the bond length. Atoms in the lattice of HEAs are usually in compressive or

tensile state by surrounding atoms due to the lattice distortion. The stress of atoms in the lattice is very local which can be empirically described by atomic level pressure [32]. The same atom have variable sizes during alloying which yields complex atomic level pressures in solid solution alloys have also been observed in FCC solid solution alloys before [32]. By comparing the error bars of bond length in Fig. s3, the error bars of the TiVNbMoTaWRe are significantly smaller than that of other alloys, which directly suggests that the local lattice distortion in the TiVNbMoTaWRe alloy is obviously smaller than that in other alloys. The result is consistent with atomic size mismatch and experimental data.

Local lattice distortion is one of the main structural characters of HEAs, which has significant effects on the mechanical and physical properties of alloys. The lattice distortion in HEAs is closely relative to both atomic size mismatch and chemical complexity. The lattice distortion can be qualitatively estimated from atomic size mismatch. However, due to the slight difference of atomic size alloying in different systems, empirical estimation is insufficient. The combination of total scattering, EXAFS measurements and first principles calculation is a powerful method to reveal the local lattice distortion quantitatively in HEAs, and our results suggest that atomic size mismatch is more critical to lattice distortion than the chemical complexity.

4. Conclusions

In summary, the local structure of the BCC solid solution alloys was studied by experimental measurements and theoretical calculations. The neutron total scattering analysis suggested that both chemical complexity and atomic size mismatch have effect on the lattice distortion in HEAs, but the latter one is more sensitive. EXAFS analysis and first principles calculation indicated that the nearest atomic pair distance strongly depends on the atomic size of elements and the size of the same atom may vary in different alloys.

Acknowledgment

Neutron diffraction measurements used resources at the Spallation Neutron Source, a DOE Office of Science User Facility operated by the Oak Ridge National Laboratory.

F. Zhang would like to acknowledge Dr Bruce Ravel for the help of EXAFS measurements, which were performed at beamlines 6-BM of the National Synchrotron Light Source II, a DOE Office of Science User Facility operated for the DOE Office of Science by Brookhaven National Laboratory under contract no. DE-SC0012704. This research was financially supported by Natural Science Foundation of China under contract numbers of 52130108 and 52173226.

References

[1] J.W. Yeh, S.K. Chen, S.J. Lin, J.Y. Gan, T.S. Chin, T.T. Shun, C.H. Tsau, S.Y. Chang, Nanostructured high-entropy alloys with multiple principal elements: Novel alloy design concepts and outcomes, Adv. Eng. Mater. 6 (2004) 299–303. https://doi.org/10.1002/adem.200300567.

[2] B. Cantor, I.T.H. Chang, P. Knight, A.J.B. Vincent, Microstructural development in equiatomic multicomponent alloys, Mater. Sci. Eng. A. 375–377 (2004) 213–218. https://doi.org/10.1016/j.msea.2003.10.257.

[3] D.B. Miracle, O.N. Senkov, A critical review of high entropy alloys and related concepts, Acta Mater. 122 (2017) 448–511. https://doi.org/10.1016/j.actamat.2016.08.081.

[4] M.H. Tsai, J.W. Yeh, High-entropy alloys: A critical review, Mater. Res. Lett. 2 (2014) 107–123. https://doi.org/10.1080/21663831.2014.912690.

[5] E.P. George, D. Raabe, R.O. Ritchie, High-entropy alloys, Nat. Rev. Mater. 4 (2019) 515–534. https://doi.org/10.1038/s41578-019-0121-4.

[6] Y. Zhang, T.T. Zuo, Z. Tang, M.C. Gao, K.A. Dahmen, P.K. Liaw, Z.P. Lu, Microstructures and properties of high-entropy alloys, Prog. Mater. Sci. 61 (2014) 1–93. https://doi.org/10.1016/j.pmatsci.2013.10.001.

[7] Y. Tong, G. Velisa, S. Zhao, W. Guo, T. Yang, K. Jin, C. Lu, H. Bei, J.Y.P. Ko, D.C. Pagan, Y. Zhang, L. Wang, F.X. Zhang, Evolution of local lattice distortion under irradiation in medium- and high-entropy alloys, Materialia. 2 (2018). https://doi.org/10.1016/j.mtla.2018.06.008.

[8] Y. Tong, S. Zhao, H. Bei, T. Egami, Y. Zhang, F. Zhang, Severe local lattice distortion in Zr- and/or Hf-containing refractory multi-principal element alloys, Acta Mater. 183 (2020) 172–181. https://doi.org/10.1016/j.actamat.2019.11.026.

[9] F. Otto, N.L. Hanold, E.P. George, Microstructural evolution after thermomechanical processing in an equiatomic, single-phase CoCrFeMnNi high-entropy alloy with special focus on twin boundaries, Intermetallics. 54 (2014) 39–48. https://doi.org/10.1016/j.intermet.2014.05.014.

[10] Z. Li, K. Pradeep, Y. Deng, D. Raabe, C. Tasan, Metastable high entropy dual-phase alloys overcome the strength-ductility trade-off, Nature. 534 (2016) 227–231.

[11] Z. Lei, X. Liu, Y. Wu, H. Wang, S. Jiang, S. Wang, X. Hui, Y. Wu, B. Gault, P. Kontis, D. Raabe, L. Gu, Q. Zhang, H. Chen, H. Wang, J. Liu, K. An, Q. Zeng, T.G. Nieh, Z. Lu, Enhanced strength and ductility in a high-entropy alloy via ordered oxygen complexes, Nature. 563 (2018) 546–550.

https://doi.org/10.1038/s41586-018-0685-y.

[12] O.N. Senkov, J.D. Miller, D.B. Miracle, C. Woodward, Accelerated exploration of multi-principal element alloys with solid solution phases, Nat. Commun. 6 (2015) 1–10. https://doi.org/10.1038/ncomms7529.

[13] Z.J. Zhang, M.M. Mao, J. Wang, B. Gludovatz, Z. Zhang, S.X. Mao, E.P. George, Q. Yu, R.O. Ritchie, Nanoscale origins of the damage tolerance of the high-entropy alloy CrMnFeCoNi, Nat. Commun. 6 (2015) 10143. https://doi.org/10.1038/ncomms10143.

[14] R.L. Fleischer, Substitutional solution hardening, Acta Met. 11 (1963) 203–209.

[15] U.F. Kocks, Kinetics of Solution Hardening, Metall. Mater. Trans. A Phys. Metall. Mater. Sci. 16 (1985) 2109–2129.

[16] M.Z. Butt, P. Felthan, Review Solid-solution hardening, J. Mater. Sci. 28 (1993) 2557–2576.

[17] F. Otto, A. Dlouhý, K.G. Pradeep, M. Kuběnová, D. Raabe, G. Eggeler, E.P. George, Decomposition of the single-phase high-entropy alloy CrMnFeCoNi after prolonged anneals at intermediate temperatures, Acta Mater. 112 (2016) 40–52. https://doi.org/10.1016/j.actamat.2016.04.005.

[18] Y. Zhang, Y.J. Zhou, J.P. Lin, G.L. Chen, P.K. Liaw, Solid-solution phase formation rules for multi-component alloys, Adv. Eng. Mater. 10 (2008) 534–538. https://doi.org/10.1002/adem.200700240.

[19] Y. Tong, S. Zhao, K. Jin, H. Bei, J.Y.P. Ko, Y. Zhang, F.X. Zhang, A comparison study of local lattice distortion in Ni80Pd20 binary alloy and FeCoNiCrPd high-entropy alloy, Scr. Mater. 156 (2018) 14–18. https://doi.org/10.1016/j.scriptamat.2018.07.002.

[20] Y. Tong, S. Zhao, H. Bei, T. Egami, Y. Zhang, F. Zhang, Severe local lattice distortion in Zr- and/or Hf-containing refractory multi-principal element alloys, Acta Mater. 183 (2020) 172–181. https://doi.org/10.1016/j.actamat.2019.11.026.

[21] Y. Tong, F. Zhang, Critical Review of Chemical Complexity Effect on Local Structure of Multi-principal-Element Alloys, JOM. 71 (2019). https://doi.org/10.1007/s11837-019-03705-3.

[22] Y. Tong, K. Jin, H. Bei, J.Y.P. Ko, D.C. Pagan, Y. Zhang, F.X. Zhang, Local lattice distortion in NiCoCr, FeCoNiCr and FeCoNiCrMn concentrated alloys investigated by synchrotron X-ray diffraction, Mater. Des. 155 (2018) 1–7. https://doi.org/10.1016/j.matdes.2018.05.056.

[23] F.X. Zhang, Y. Tong, K. Jin, H. Bei, W.J. Weber, A. Huq, A. Lanzirotti, M. Newville, D.C. Pagan, J.Y.P. Ko, Y. Zhang, Chemical complexity induced local structural distortion in nicofemncr high-entropy alloy, Mater. Res. Lett. 6 (2018) 450–455. https://doi.org/10.1080/21663831.2018.1478332.

[24] F.X. Zhang, Y. Tong, M. Kirkham, A. Huq, H. Bei, W.J. Weber, Y. Zhang, Structural disorder, phase stability and compressibility of refractory body-centered cubic solid-solution alloys, J. Alloys Compd. 847 (2020) 155970. https://doi.org/10.1016/j.jallcom.2020.155970.

[25] P. Juhás, T. Davis, C.L. Farrow, S.J.L. Billinge, PDFgetX3: A rapid and highly automatable program for processing powder diffraction data into total scattering pair distribution functions, J. Appl. Crystallogr. 46 (2013) 560–566. https://doi.org/10.1107/S0021889813005190.
[26] B. Ravel, M. Newville, ATHENA, ARTEMIS, HEPHAESTUS: Data analysis for X-ray absorption spectroscopy using IFEFFIT, J. Synchrotron Radiat. 12 (2005) 537–541. https://doi.org/10.1107/S0909049505012719.
[27] P.E. Blöchl, Projector augmented-wave method, Phys. Rev. B. 50 (1994) 17953–17979. https://doi.org/10.1103/PhysRevB.50.17953.
[28] J.P. Perdew, K. Burke, M. Ernzerhof, Generalized Gradient Approximation Made Simple, Phys. Rev. Lett. 77 (1996) 3865–3868. https://doi.org/10.1103/PhysRevLett.77.3865.
[29] F. Tian, D.-Y. Lin, X. Gao, Y.-F. Zhao, H.-F. Song, A structural modeling approach to solid solutions based on the similar atomic environment, J. Chem. Phys. 153 (2020) 034101. https://doi.org/10.1063/5.0014094.
[30] F.X. Zhang, S. Zhao, K. Jin, H. Xue, G. Velisa, H. Bei, R. Huang, J.Y.P. Ko, D.C. Pagan, J.C. Neuefeind, W.J. Weber, Y. Zhang, Local Structure and Short-Range Order in a NiCoCr Solid Solution Alloy, Phys. Rev. Lett. 118 (2017). https://doi.org/10.1103/PhysRevLett.118.205501.
[31] H. Song, M. Yu, Y. Zhang, W. Zhang, Z. Liu, F. Zhang, F. Tian, First-principle study of interstitial atoms (c,B and Si) in CrFeCoNi high entropy alloy, Mater. Today Commun. 31 (2022) 103241.
[32] H.S. Oh, S.J. Kim, K. Odbadrakh, W.H. Ryu, K.N. Yoon, S. Mu, F. Körmann, Y. Ikeda, C.C. Tasan, D. Raabe, T. Egami, E.S. Park, Engineering atomic-level complexity in high-entropy and complex concentrated alloys, Nat. Commun. 10 (2019) 2090. https://doi.org/10.1038/s41467-019-10012-7.
[33] M. Yu, D.R. Trinkle, Accurate and efficient algorithm for Bader charge integration, J. Chem. Phys. 134 (2011) 064111. https://doi.org/10.1063/1.3553716.

Figure Captions

Fig. 1 (a) The crystal structure model and (b) the pair correlation function of VNbTa solid solution alloy. The 3 x 3 x 3 supercell model, containing 54 atoms, has selected for DFT calculation. The atomic positions have optimized by the SAE method. r_0 is the first nearest neighbor distance.

Fig. 2 The atomic pair distribution function analysis of VNbTa measured with time-of-flight neutron scattering a) the PDF profiles in the whole r-range (1.5-30 Å) is fitted with a randomly distributed bcc structure model, and the first two peaks are not well fitted; b) The fitting is improved by split the whole profile into 3 different regions: local (within one unit cell), intermediate region (1-3 unit cells: 4-10 Å) and long-range (>10 Å)

Fig. 3 The atomic pair distribution function analysis of TiVNbMoTaWRe measured with time-of-flight neutron scattering a) The PDF profiles in the whole r-range (1.5-30 Å) is fitted with a randomly distributed bcc structure model, and the first two

p□aks ar□not w□ll fitt□d; b) Th□fitting is improv□d by split th□whol□profil□into 3 different regions: local (within one unit cell), intermediate region (1-3 unit cells: 4-10 Å) and long-range (>10 Å)

Fig. 4 The local lattice strain in the solid-solution alloys derived from PDF fitting

Fig. 5 The fitting of FTs of EXAFS at the K-edge of V and Nb and L_3-edge of Ta in VNbTa solid-solution alloy

Fig. 6 Distance of atomic pairs in VNbTa ternary solid solution alloy obtained by EXAFS measurement and first principles calculation

Table 2 The distance of atomic pairs in HEAs from fitting of FTs of EXAFS profiles

Alloy	V(Ti)-core k ($Å^{-1}$), R (Å) d (Å)	Nb(Mo)-core k ($Å^{-1}$), R (Å) d (Å)	Re(W,Ta)-core k ($Å^{-1}$), R (Å) d (Å)
VNbTa	*k: 3-11, R: 1.25-5* V-V: 2.77 (9) V-Nb: 2.78 (9) V-Ta: 2.77 (9)	*k: 2.4-12, R: 1.25-5* Nb-V: 2.74 (12) Nb-Nb: 2.81(6) Nb-Ta: 2.88 (2)	*k: 3.6-14, R: 1.5-5* Ta-V: 2.85 (1) Ta-Nb: 2.86 (1) Ta-Ta: 2.85 (1)
TiVNbMo	*k: 3-12, R: 1.25-3* V-V (Ti): 2.75 (2) V-Nb (Mo): 2.75 (2) *k: 3-11, R: 1.25-3* Ti-V (Ti): 2.85 (12) Ti-Nb (Mo): 2.83 (9)	*k: 3-12, R: 1.25-3* Nb-V (Ti): 2.79 (6) Nb-Nb (Mo): 2.80 (7) *k: 3-11, R: 1.25-3* Mo-V (Ti): 2.74 (1) Mo-Nb (Mo): 2.75 (3)	
TiVNbMoTa	*k: 3-12, R: 1.25-3* V-V (Ti): 2.69 (4) V-Nb (Mo): 2.80 (7) V-Ta: 2.73 (1)	*k: 3-14, R: 1.25-3* Nb-V (Ti): 2.731 (3) Nb-Nb (Mo): 2.80 (8) Nb-Ta: 2.82 (9)	*k: 3-11, R: 1.25-3* Ta-V (Ti): 2.77 (4) Ta-Nb (Mo): 2.81 (8) Ta-Ta: 2.83 (10)
TiVNbMo-TaWRe	*k: 3-13, R: 1.25-3* V-V (Ti): 2.67 (7) V-Nb (Mo): 2.74 (1) V-Ta (W, Re): 2.72 (3)	*k: 3-14, R: 1.25-3* Nb-V (Ti): 2.70 (4) Nb-Nb (Mo): 2.78 (3) Nb-Ta (W, Re): 2.77 (2) *k: 3-12.5, R: 1.25-3* Mo-V (Ti): 2.57 (17) Mo-Nb (Mo): 2.77 (2) Mo-Ta (W, Re): 2.75 (1)	*k: 3-11, R: 1.25-3* Re-V (Ti): 2.59 (15) Re-Nb (Mo): 2.76 (1) Re-Ta (W, Re): 2.74 (1)

Figure 1

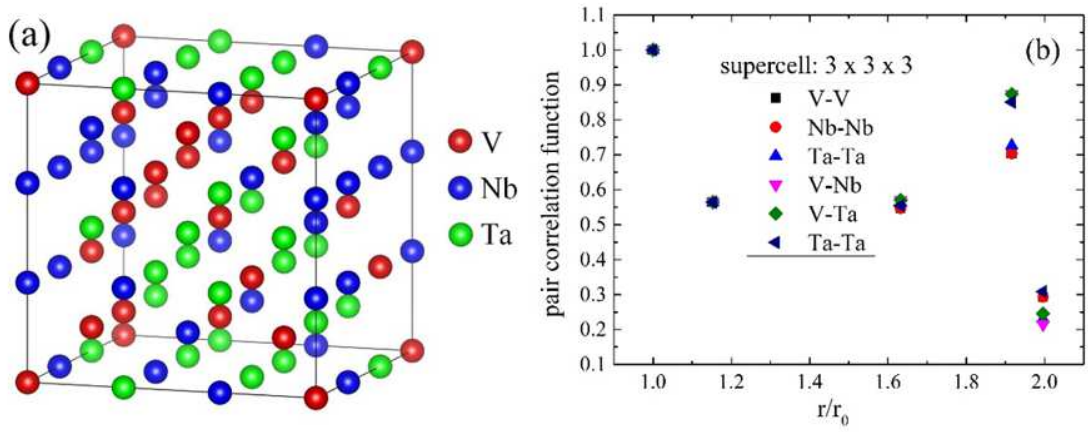

Figure 2

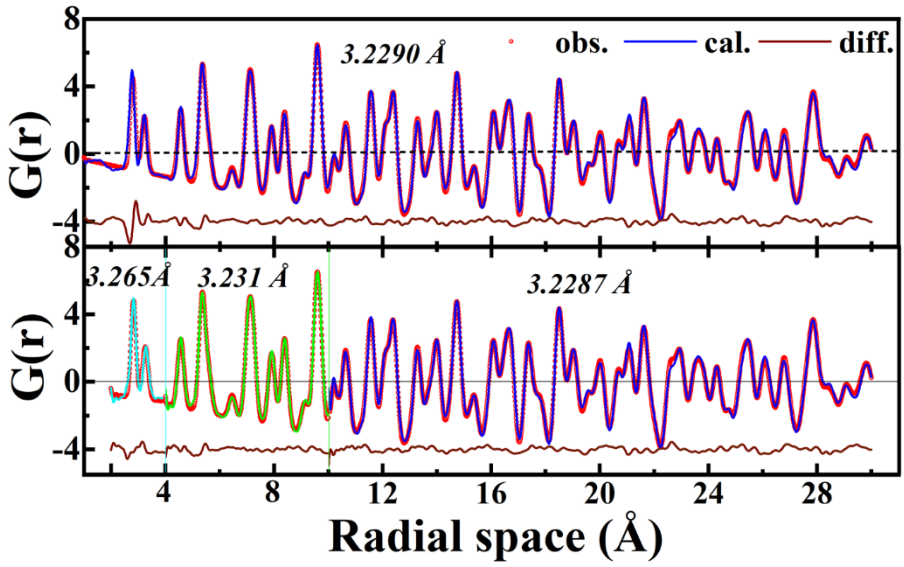

Figure 3

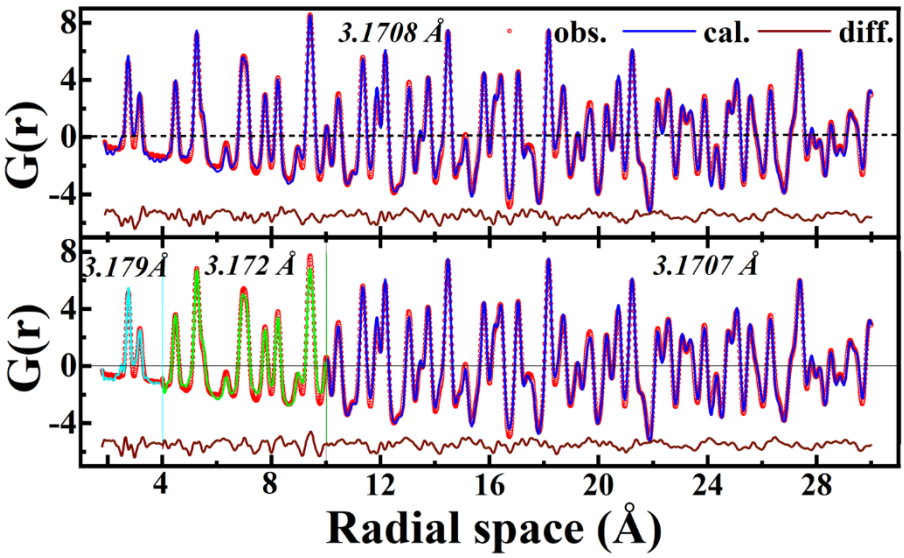

Figure 4

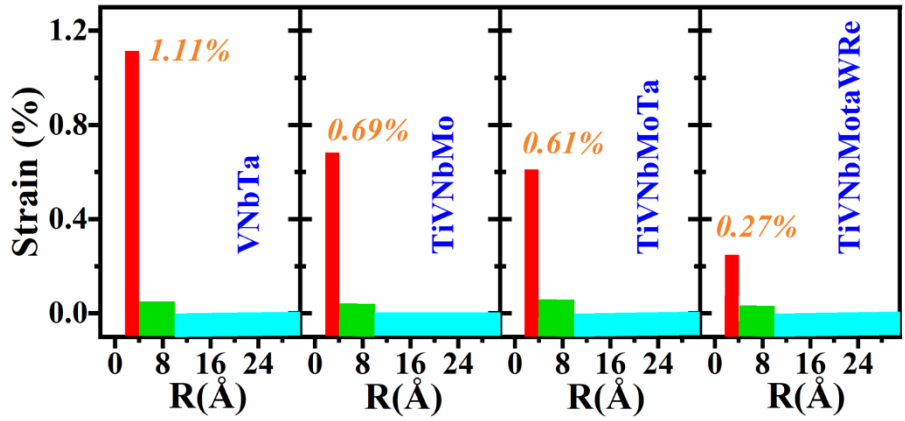

Figure 5

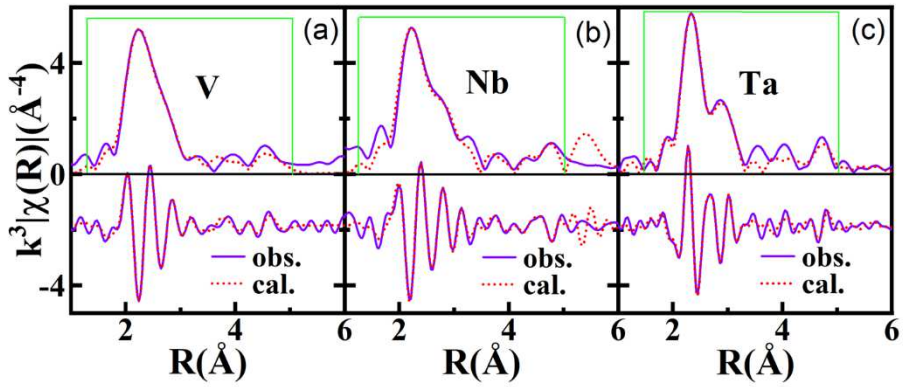

Figure 6

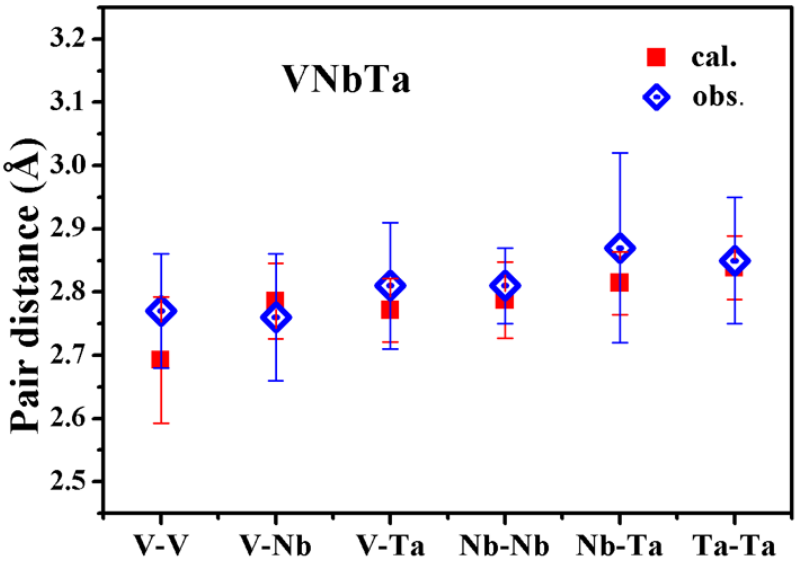

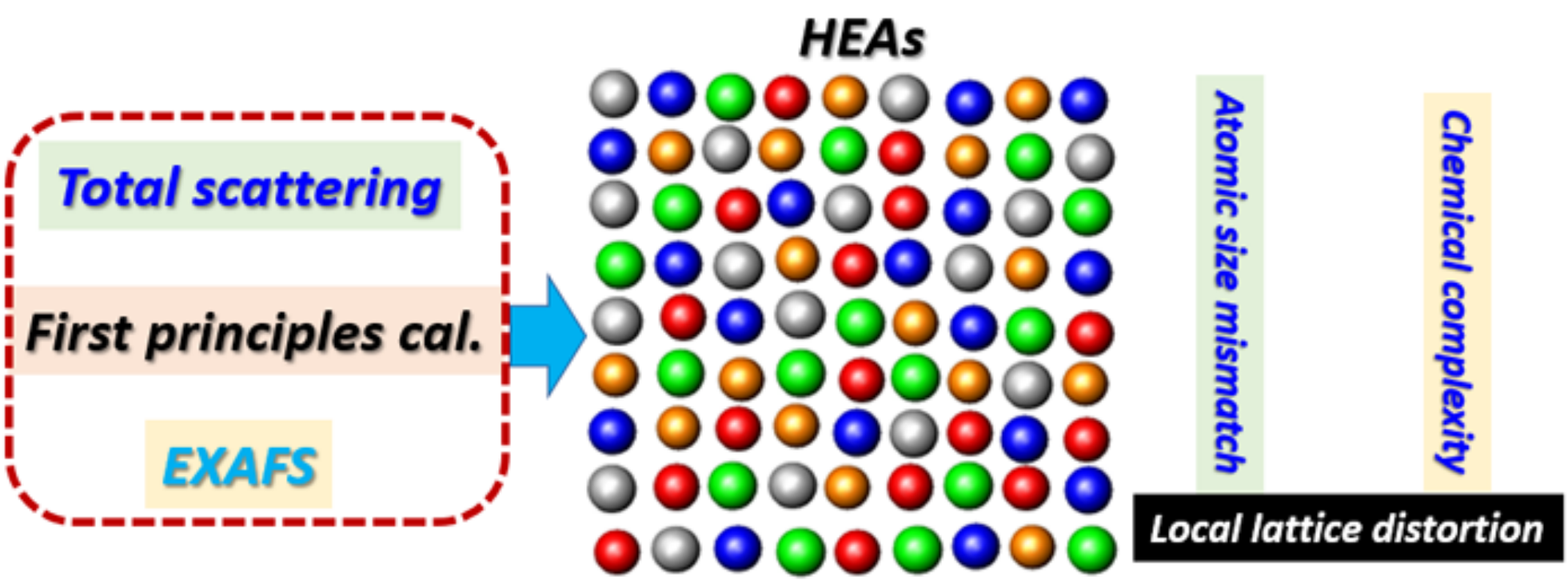
Total scattering
First principles cal.
EXAFS
HEAs
Atomic size mismatch
Chemical complexity
Local lattice distortion